

## Chapter 7

### Development of FD-OCT system employing LED and a Webcam

#### 7.1 Introduction

The primary goal of medical imaging is to produce images for diagnostic or screening purpose which leads to a finer understanding of pathogenesis consequently leading to contribution in the development of effective patient care and course of the treatment. In the past couple of decades, minimally invasive radiological techniques such as X ray [324], computerized tomography (CT) [325], magnetic resonance imaging (MRI) [326], radioisotope imaging (positron emission tomography) [327] etc have brought significant transformation in medical research and clinical practice. These techniques enables one to have a three-dimensional visualization but with a limited spatial resolution (few millimetres in conventional clinical practices) [328,329]. On the other hand, optical imaging techniques hold key importance in number of scientific disciplines especially in the field of biomedical imaging as these techniques provide numerous advantages over radiological imaging techniques and are used to obtain three-dimensional (3D) high-resolution images of organs, tissues, cells and molecules using visible light with the ability to improve treatment, diagnosis and prevention of diseases [330–333]. One of the major benefits that 3D image dataset offers is flexible image visualization capability. The target tissue can be sliced in any random plane thereby letting the clinicians to examine the anomalies from different vantage points [153,328,334,335].

The technological and scientific collaboration between physicists and clinicians has led to development of Optical Coherence Tomography (OCT). It is a rapidly emerging, robust, non-invasive, 3D sub surface tissue imaging technique [162]. OCT is an optical analog to ultrasound technique which achieves two or three dimensional cross sectional images of tissue and works on the property of tissues to reflect and back scatter light involving low coherence interferometry [155,329,336–347]. As the resolution is getting refined, the identification, detection, localization and quantification of tissue has become more reliable and advanced. OCT is efficient in generating high resolution, cross-sectional images of non-uniform specimen such as biological tissues with attractive features such as high cellular resolution, real time acquisition rate etc [161,162,328,334,335,340,348–351]. It provides both qualitative (morphological) as well as quantitative (thickness mapping and volume) analysis of the tissue under examination in real time [350].

Ever since its inception in the 1990s, OCT has been adopted successfully in many fields especially in biomedical imaging to perform 3D in vivo optical biopsy non-invasively with fine resolution in both lateral and axial dimensions at a penetration depth up to few millimetres [335,341,344,345]. Some of the remarkable qualities of OCT are (i) High resolution images (OCT has been known to furnish images (axial resolution of the range of 1-10 $\mu$ m) [351,352] (ii) Rapid imaging speed (providing temporal resolution up to milliseconds) [351,353] (iii) Label free imaging (providing fine images without any need of contrast agent) [351,354,355] (iv) Additional functionality (along with rendering depth resolved structural images of the sample under study), OCT can also furnish further information such as blood flow through Doppler OCT, tissue structural arrangement through birefringence OCT [351,352] etc. These unique qualities have helped OCT technique gain popularity within a short span of time. These aforementioned qualities make OCT a potential tool to explore various clinical applications that will enhance current imaging techniques. It will also aid in revealing previously difficult to observe structural and functional changes in the tissue under investigation. The initial application was imaging of biological tissue [162,356] and most notably in the field of ophthalmology where diagnostic imaging was carried out on the transparent structures of the anterior of the eye [162,329,344,357–361]. OCT has also been used in many of the major systems of humans such as cardiology [344,362–367], gastroenterology [162,368–372], urology [162,344,373–377], dermatology [344,378–381], dentistry [344,382–384], oncology [344,385,386], pulmonary [344,387], fingerprint detection [388,389] to name a few. OCT has also been demonstrated in biological sciences including neurobiology [162,390–392]. It has also been employed for the visualization of processes such as mitosis and cell migration [162,393,394]. There are various non biological application of OCT as well which includes non-destructive evaluation of polymers, ceramics and coatings [162,395,396]. It has also been utilized to optically interpret digital data from multilayer optical disk [162,397]. Optical ranging is a technique performed by OCT, that is used in the telecommunications industry to locate defects in optical fibres that make up an optical communication network. [162,398].

OCT is primarily based on low coherence interferometry employing Michelson interferometer (Fig. 7.1) [161,335,357] and its performance inherently depends on the light source used [161,346]. The most important criterion for the selection of the light source in OCT is its wavelength which should be in the Near Infrared (NIR) region. Moreover, it should have a broad bandwidth, high power in single transverse mode (high irradiance) and short temporal coherence length [346]. The reason for the source to emit in the NIR region is to ensure that

adequate amount of light is penetrated into the tissue. The second reason for the high irradiance is that imaging weakly backscattering structures deep in the tissue necessitates a high dynamic range and detection sensitivity. The basis for the third condition of the short coherence length is to achieve better axial resolution and contrast [346]. The commercial standard-resolution OCT instruments employ super luminescent diodes (SLD) which mainly emit 20-30nm bandwidths with central wavelength at 830nm [357]. Instead of traditional SLD light sources, a state-of-the-art, ultrabroad-bandwidth, solid state femto-second Ti:sapphire lasers have also been employed. This laser is combined with photonic crystal fibres that exhibit strong dispersion so that the spectral bandwidth of the light emitted at the end of the fibre is increased [399]. Femtosecond laser technology has attained remarkable performance in image resolution but offers certain disadvantages such as it is expensive and lack of portability, thus limiting its use in fundamental research [357]. Advanced SLD light sources which are comparatively cost effective have become available that reach the image resolution that is offered by femtosecond lasers [162,400,401]. These light sources are multiplexed SLDs, which are combined of two or three spectrally displaced SLDs that create a broad spectrum. Multiplexed SLDs are less expensive and more durable than femtosecond lasers, but they have the disadvantage of spectrally modulated emission spectra, which causes imaging artefacts due to axial point spread function. Therefore, there always remains a trade-off between cost and performance [357].

This chapter describes the design and development of a low-cost Fourier Domain Optical Coherence Tomography (FD-OCT) system which employs a Light Emitting Diode (LED) due to its relative simplicity, compactness, robustness and low cost, instead of Super luminescent Diode (SLD) that is the standard light source used in commercially available OCT devices and a webcam instead of a high-end detector. For the proof of concept, the object that is used are mirrors which are etched and mirrors that are kept at different depths.

## **7.2 Basic theory of Optical Coherence Tomography**

OCT is based on the principal of coherence gating which requires temporal and spatial overlap of the light reflected from the investigated sample and a reference beam to produce interference within the tolerance of the source coherence length [334,371]. OCT relies on ballistic and near ballistic photons but since the number of ballistic photons decay exponentially with the propagation distance which requires optical heterodyning to detect weak ballistic signals and achieve shot-noise limited detection [161,335,402]. OCT works on interferometric detection techniques since the velocity of light is very high hence, the time delay of reflected light cannot

be determined directly, unlike Ultrasound which works on determining the time delay of the reflected sound wave [403]. OCT is a coherence gated technique which uses low coherence interferometry carried out using Michelson type interferometer (Fig. 7.1) [6, 11, 13, 14, 20, 28, 38, 72, 82].

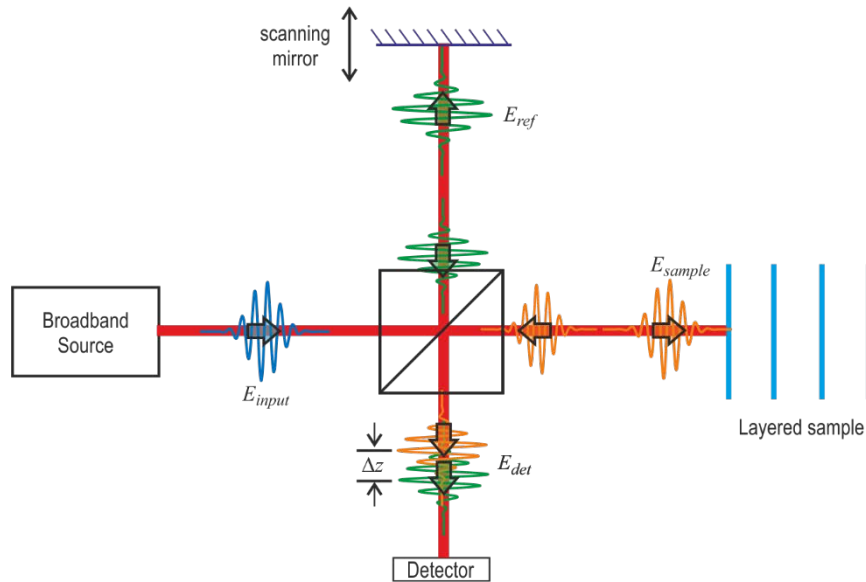


Fig 7.1 General OCT system based on a Michelson interferometer

Light from the optical source is split into two beams with the help of a BS. One beams travels towards the reference mirror arm and the other travels towards the object arm of the interferometer. The beams reflected from the reference mirror and the different layers within the objects are later superposed at the detector to produce interference fringes for which the condition is that the path length between both the beams should match. The reference mirror is shifted to alter the reference path length so as to match multiple optical paths due to reflection within the sample. The position of the reference mirror determines the depth in the sample from which the magnitude of reflection is measured. The intensity peaks in the interference pattern are an indication of the sharp RI variation within the sample [161,162,334,335,345,362,395,405].

### 7.3. Theoretical formulation

For theoretical formulation of OCT, the complex exponential notation of the electric field  $E(\omega, t)$  is used [161]

$$E(\omega, t) = s(\omega) \exp[-i(\omega t + kz)] \tag{7.1}$$

Eq. (7.1) describes a solution to the wave equation where  $s(\omega)$  represents amplitude spectrum of the source (amplitude as a function of frequency  $\omega$ ). In Eq. (7.1) wave number is denoted by  $k$  and the distance denoted by  $z$  is the path length followed by the light beam in the interferometer, with  $kz$  denoting phase amassed. The interferometer measures the difference in the phase of the two interfering beams [161].

The terms  $E_{input}$ ,  $E_{ref}$ ,  $E_{sample}$ ,  $E_{det}$  (Fig. 7.1) denotes the optical field in the input, reference arm, sample arm and at the detector respectively. Here it is assumed that the reference mirror is ideal and  $T_r$ ,  $T_s$  denote the reference and sample arm intensity transmittance.

$$E_{input}(\omega, t) = s(\omega)e^{-i\omega t} \quad (7.2)$$

$$E_{ref}(\omega, t, \Delta z) = (T_r T_s)^{1/2} E_{input}(\omega, t) e^{-i\phi(\Delta z)} \quad (7.3)$$

$$E_{sample}(\omega, t) = (T_r T_s)^{1/2} E_{input}(\omega, t) H(\omega) \quad (7.4)$$

$$E_{det}(\omega, t, \Delta z) = E_{ref}(\omega, t) + E_{sample}(\omega, t, \Delta z) \quad (7.5)$$

where  $H(\omega)$  is the sample frequency domain response function.  $\phi(\Delta z)$  denotes the phase accumulation (due to path length difference between sample and reference beam) while translating the mirror by distance  $\Delta z = \Delta t / n_{air}$

$$\phi(\Delta z) = \frac{2\omega n_{air} \Delta z}{c} \quad (7.6)$$

The optical time of flight difference is given by  $\Delta t$ , speed of light is denoted by  $c$ , while the group RI of the air is denoted by  $n_{air}$  [161].

Optical sensors can register only intensity (absolute square of light complex amplitude). The recorded intensity ( $I_{det}$ ) is proportional to the time average of the absolute square of the light electric field distribution given by:

$$I_{det}(\omega, \Delta z) = \langle E_{det}(\omega, t, \Delta z) E_{det}^*(\omega, t, \Delta z) \rangle \quad (7.7)$$

Substituting Eq. (7.5) into Eq. (7.7), it can be concluded that the intensity is a sum of 3 terms:

$$I_{det}(\omega, \Delta z) = \langle E_{sample} E_{sample}^* \rangle + \langle E_{ref} E_{ref}^* \rangle + 2\Re\{\langle E_{sample} E_{ref}^* \rangle\} \quad (7.8)$$

The first 2 terms are called background whereas the interference term is denoted by the last term of the equation (due to the superposition of sample and reference waves)

Making substitutions from Eq. (7.2) to (7.4) and using intensity spectrum  $S(\omega) = |s(\omega)|^2$ , the frequency and path difference ( $\Delta z$ ) dependent intensity at the detector is given by [161]

$$I_{det}(\omega, \Delta z) = T_r T_s S(\omega) |H(\omega)|^2 + T_r T_s S(\omega) + 2T_r T_s \Re\{S(\omega) H(\omega) e^{-i\phi(\Delta z)}\} \quad (7.9)$$

The sample response function denoted by  $H(\omega)$  describes the overall reflection from all the structures, considering the reflection coefficient of the structures inside the sample as well as the optical path length of the sample beam and is represented by

$$H(\omega) = \int_{-\infty}^{\infty} r(\omega, z) e^{i2n(\omega, z)\omega z/c} dz \quad (7.10)$$

The function  $r(\omega, z)$  describes the reflection coefficient (frequency dependent) of the different sample structural features, and  $n(\omega, z)$  represents the frequency dependent, depth varying group RI. From Eq. (7.9), it can be inferred that information about the optical structures of the sample can be acquired from both the time and frequency domains.

### 7.3.1 Time Domain OCT

The earliest form of OCT arrangement uses Time Domain geometry to extract depth information (Fig. 7.1). In TDOCT a reference mirror is scanned to match the optical path from reflections from the different sample structures [161,362]. To obtain the detected intensity value, Eq. (7.9) can be written as function of the path displacement of the reference beam by integrating over the source spectrum. It is assumed that beam splitter used is loss less and  $T_s=T_r=0.5$ .

Therefore, the interference pattern obtained in TDOCT from each scan can be given as sum of the two terms [161].

$$I_{det}(\Delta z) = \Gamma_0 + \Re\{\Gamma(\Delta z)\} \quad (7.11)$$

$\Gamma_0$  includes contribution only from background terms arising due to self-interference.

$$\Gamma_0 = \frac{1}{4} \int_{-\infty}^{\infty} S(\omega) (|H(\omega)|^2 + 1) d\omega \quad (7.12)$$

$\Gamma(\Delta z)$  has contribution only from superposition of sample and reference beams (cross-interference).

$$\Gamma(\Delta z) = \frac{1}{2} \int_{-\infty}^{\infty} H(\omega) S(\omega) \cos\{\phi(\Delta z)\} d\omega \quad (7.13)$$

The continuous sample integral can be written as a summation over N individual layers to model a simple layered sample with negligible dispersion [28]:

$$H = \sum_{j=1}^N r_j \exp\left(i2\frac{\omega}{c} \sum_{m=1}^j n_m z_m\right) \quad (7.14)$$

$z_m$  is the thickness of the  $m^{\text{th}}$  layer with a group RI  $n_m$ . Assuming normally incident light is, the reflectance, according to Fresnel equation, is given by

$$r_j = \frac{n_{j+1} - n_j}{n_{j+1} + n_j} \quad (7.15)$$

### 7.3.2 Fourier Domain OCT

In Fourier domain OCT (FD-OCT) the detected intensity spectrum which is recorded using a spectrometer is Fourier transformed into the time domain to reconstruct the depth resolved

sample optical structures [161,339] hence, does not require any moving parts to obtain axial scans.

Eq. (7.9) is also true for FD-OCT. Since reference mirror is not moving,  $|\Delta z|=0$  (or constant and less than the coherence length of the source) and assuming that the beam splitter (BS) is ideal with 50:50 ratio the expression for the recorded frequency spectrum is [161].

$$I(\omega) = \frac{1}{4} S(\omega) \{H(\omega) + 1\}^2 \quad (7.16)$$

By dividing the recorded intensity spectrum (spectral interference pattern) by the measured source spectrum, an arbitrary source spectrum can be deconvolved from the sample response.

The depth resolved structural data is reconstructed by Fourier Transforming  $I(\omega)$  into the time domain interference pattern  $I(t)$ .

$$I(t) = FT \{I(\omega)\} \quad (7.17)$$

In Eq. (7.17), the Fourier Transform operation is denoted by FT. The interference pattern can be plotted as a function of reference mirror displacement  $\Delta z$  and optical time of flight  $t$ .

In a practical system,  $I(\omega)$  (output intensity spectrum) recorded by an arrayed detector is a set of  $N$  discrete data points each corresponding to an intensity measured by each detector point on the array. The easiest way to compute FT of the recorded spectrum is using Fast Fourier Transform (FFT) algorithm. The resulting FT is composed of a series of  $N/2$  discrete steps in time  $\Delta\tau$  determined by the detected source spectral width  $\Delta\Omega$  [161].

$$\Delta\tau = \frac{2\pi}{\Delta\Omega} \quad (7.18)$$

The following equation can be used to approximate the detected spectrum

$$\Delta\Omega = 2\pi c \frac{\Delta\lambda}{\lambda^2} \quad (7.19)$$

Both the sides of Eq. (7.18) are multiplied by  $c/n_{ave}$  to achieve the conversion into the spatial domain, where it is assumed that  $n_{ave}$  is the average sample RI. The maximum detectable depth denoted by  $z_{max}$  is determined by multiplying Eq. (7.19) by the number of time domain points  $N/2$  and dividing by 2 considering that the light passes through the sample twice.

$$z_{max} = \frac{1}{4n_{ave}} \frac{\lambda_0^2}{\Delta\lambda} N \quad (7.20)$$

#### 7.4 Experimental Setup

The work presented in this section describes the development of a low cost FDOCT system (Fig. 7.2 and 7.3) employing LED instead of high-end optical sources like SLDs and fibre

coupled diodes and webcam instead of CCD. Light source used is a 2W Lumilex LED emitting at central wavelength  $\lambda_0 = 636$  nm and bandwidth  $\Delta\lambda=20$  nm (Fig. 7.4 shows the spectrum of the source LED) having coherence length of  $\sim 18$  micrometres (which is given by  $l_c=0.88 \lambda_0^2/\Delta\lambda$ ). to convert it into a point source (as well as increase in spatial coherence). After the pinhole light is then collimated using a spherical lens of 2.5 cm in diameter and 5cm of focal length. This collimated light beam is then directed to the beam splitter which splits the beam into two. The reflected beam acts as a reference and second beam (transmitted) acts as the object beam. Reference arm light is focused on the reference mirror (or dielectric material) by the cylindrical lens of 40 mm of focal length. Sample arm light is also focused on to the object using a cylindrical lens 40 mm of focal length to making a line of light falling on the object. Use of cylindrical lens makes a line of source light and helps in reducing the number of scans (compared to point source of object illumination). Reflected light from the reference arm and from the different depths of the sample travel back and passes through variable slit with 1mm opening. The superposed object and reference beam are then converted into the corresponding frequency spectrum using a grating of 300 lines/mm. It is then imaged on to a webcam (VGA, Intex 8-bit, 3.2  $\mu\text{m}$  pixel pitch) by the spherical lens of 5 cm in diameter and focal length of 10 cm. Spectral interference pattern is obtained if and only if the path length difference between both the arms of the interferometer is within the coherence length of the source. This spectral interference pattern corresponds to light reflected from different depths of the sample. This obtained interference pattern is in the frequency (or wavelength) domain. To convert this into the spatial domain FT of the spectral interference pattern is computed. In the experiments, object used is a mirror in which 3 holes are etched and two mirrors are kept at different distances behind the first mirror with holes and they at act as objects at different depths. Schematic of the investigated Fourier domain OCT is shown in Fig 7.2 and actual experimental setup is shown in Fig 7.3.

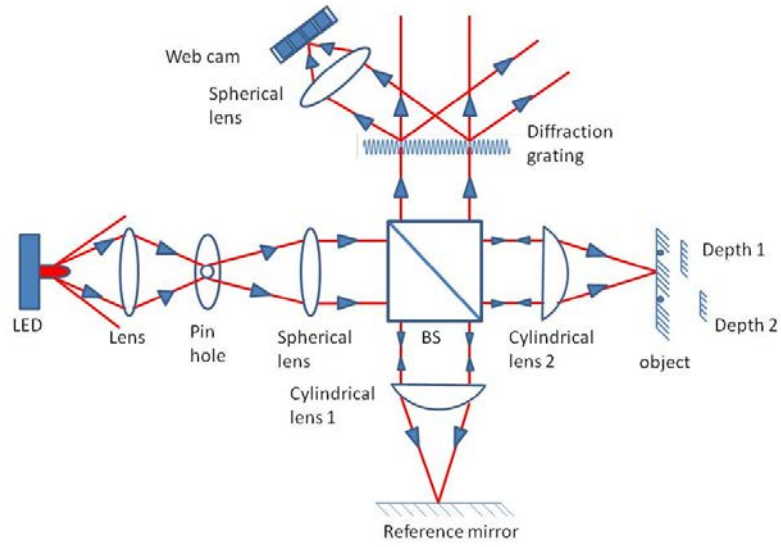


Fig 7.2 Schematic of the developed FDOCT system

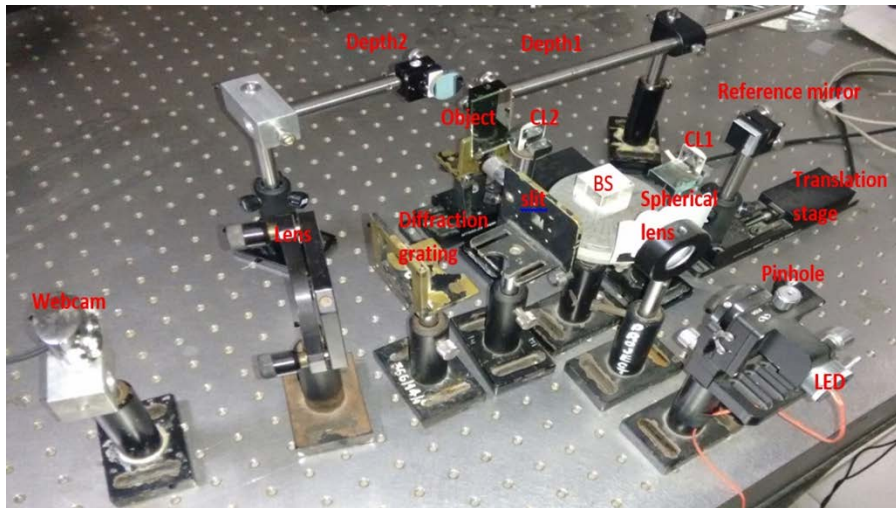


Fig 7.3 Experimental setup of FDOCT

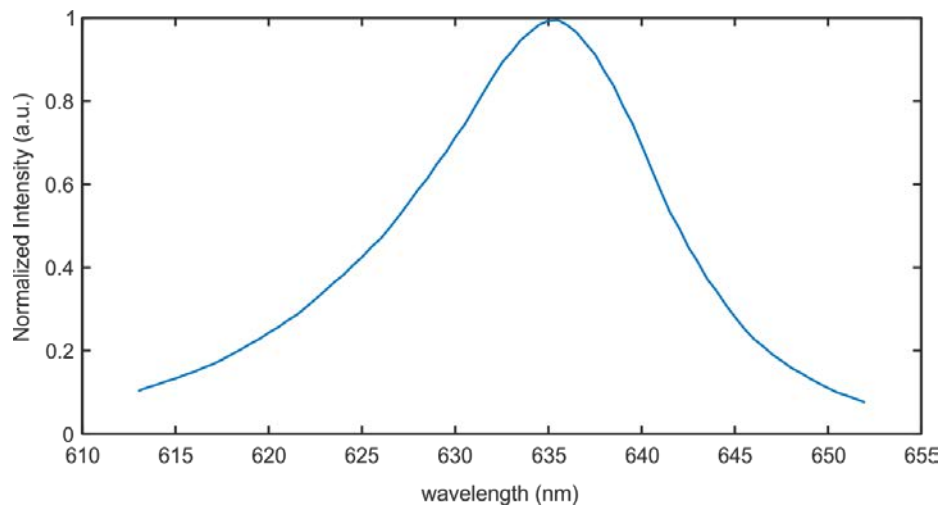


Fig 7.4 Spectrum of the LED source used in the experiments

## 7.5 Result and discussion

Developed low-cost OCT setup uses high power LED instead of SLD so it is necessary to measure the optical detection sensitivity and noise level of system. SNR is computed by capturing the spectrum of sample beam when perfectly reflecting mirror was kept at the sample arm and the ratio of the square of mean to the square of standard deviation of pixel intensity over certain region gives  $P_{SNR}$  of the system. Optical detection sensitivity is calculated by ten times logarithm of square root of SNR which is found out to be nearly 30 dB.

One of the main aspects of FDOCT is its axial resolution which decides its applications towards various areas. The source properties determine the axial resolution of the FDOCT system. The source used here is LED with coherence length of  $18\mu\text{m}$  so axial resolution is calculated to be  $9\mu\text{m}$ . The size and aperture of cylindrical slit illuminated on the object decides the lateral resolution of the system. Lateral resolution is measured experimentally be  $12\mu\text{m}$ .

The maximum detectable depth ( $z_{\text{max}}$ ) depends on the size of detector array, grating, and pixel pitch of the sensor and width of the sensor array. Experiments used a  $640 \times 480$  (VGA) webcam sensor. The number of wavelengths that can be seen by detector depends on the width of lines formed by the imaging lens on the sensor which is measured experimentally and is  $32\mu\text{m}$ . Each discrete wavelength covers 10 pixels on the sensor as the pixel pitch is  $3.2\mu\text{m}$ . So the number of discrete wavelength (N) is the detector array size (640 pixels) divided by the number of pixels occupied on the array by a wavelength.

To test the imaging capability of the system it is tested it in different ways. The objects used included (i) a single mirror moved axially, (ii) two mirrors at different axial positions and scanned laterally and (iii) object realized using an etched mirror (mirror with holes at different lateral positions) and mirrors kept at different axial planes behind simulating objects at different depths.

### 7.5.1 Axial scanning of a mirror

To test the depth imaging capability of the developed OCT setup initially a mirror is in the axial direction (similar to that used for TDOCT systems) in the steps of  $10\mu\text{m}$  up to  $150\mu\text{m}$  and acquired the spectral interference patterns. In this case object is not scanned in lateral direction, position of illuminating cylindrical linear source is same with respect to lateral direction. Fig. 7.5a shows the recorded spectral intensity pattern when there is no path length delay between both object and reference beams. Fig. 7.5b shows the variation in intensity for same interference pattern along the line shown in Fig. 7.5a.

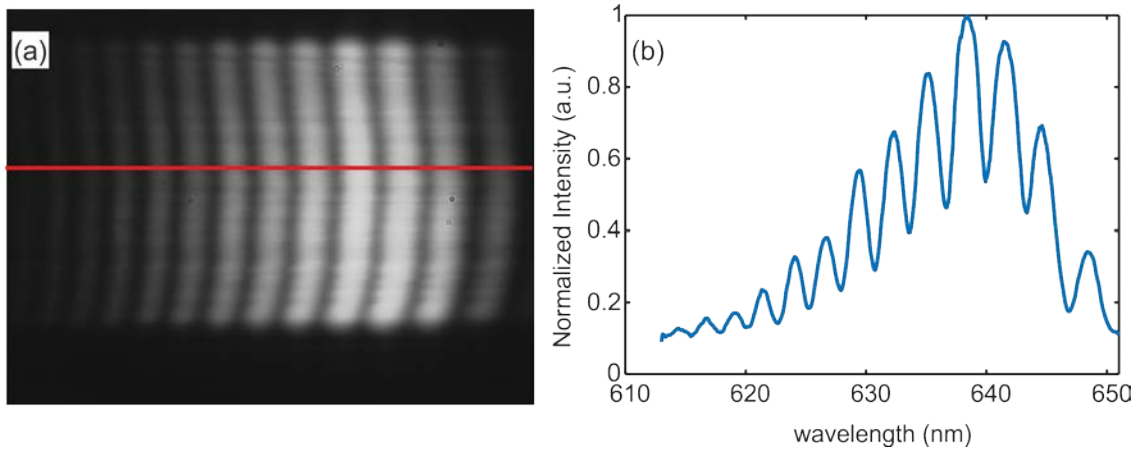


Fig 7.5 (a) Recorded spectral interference pattern for 10 $\mu$ m path length delay between object and reference paths  
 (b) Intensity profile along the line shown in Fig. 7.5a

Fig. 7.6 represents the spectral interference patterns at each 20 $\mu$ m step size. Fourier transform of the spectral interference patterns (along each column, which is the direction of variation of intensity) reconstructs the depth information of the slit at the spatial location (represented by the row number). The depth information for the whole slit is reconstructed in the similar way. Reconstructed information for different axial position of the scanning mirror is shown in Fig. 7.6

Depth separation can be easily seen in Fig 7.7 which plots the absolute of the Fourier transform of the spectral interference pattern along the horizontal line shown in Fig. 7.6. Each peak in Fig 7.7 corresponds to the 10 $\mu$ m translation of scanning mirror. Peak at  $\Delta z = 0$  correspond to the FT of source spectrum.

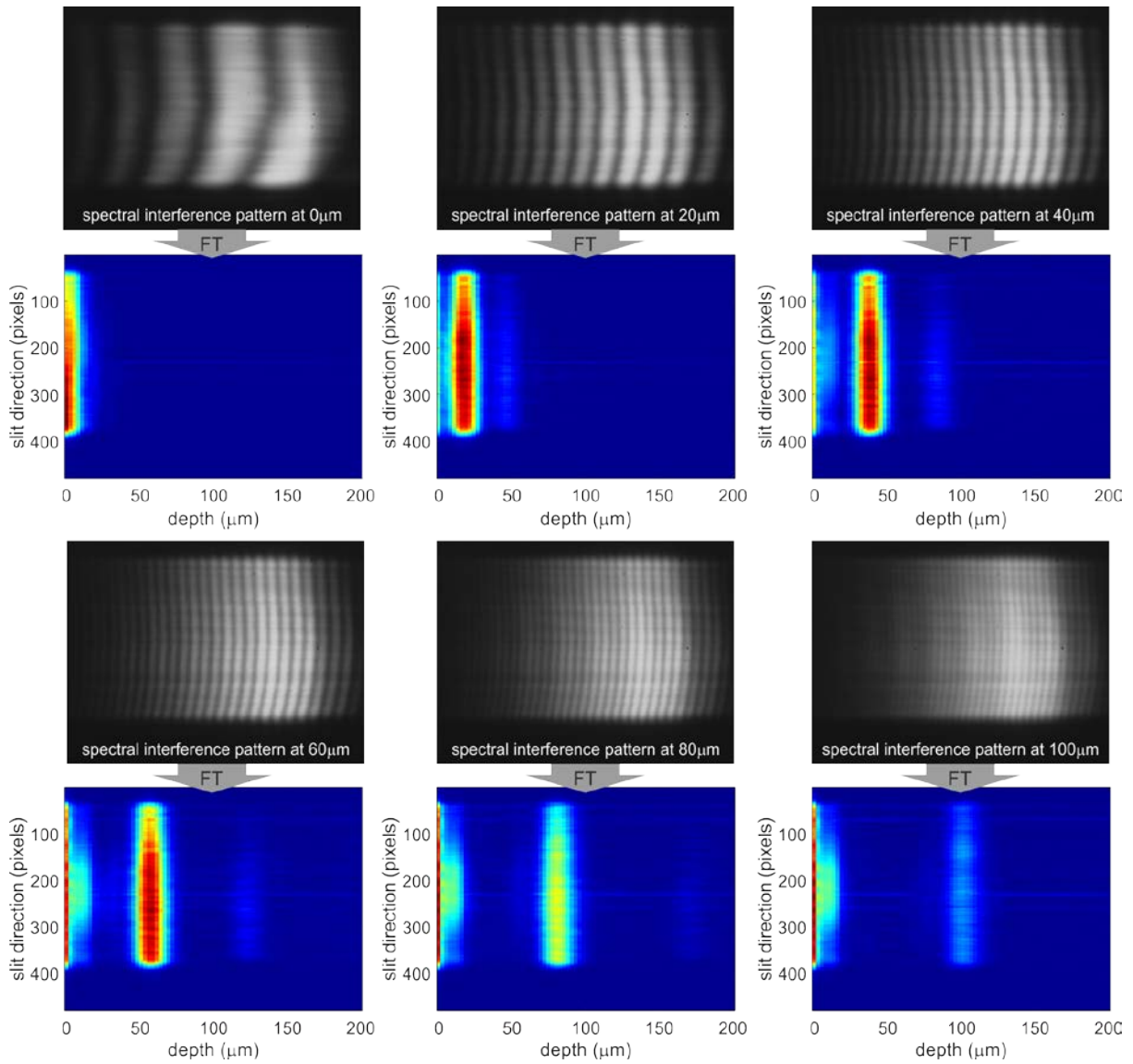


Fig 7.6 Recorded spectral interference patterns at different axial positions of the scanning mirror and the reconstructed depth profiles by Fourier Transforming the intensity profile along each column

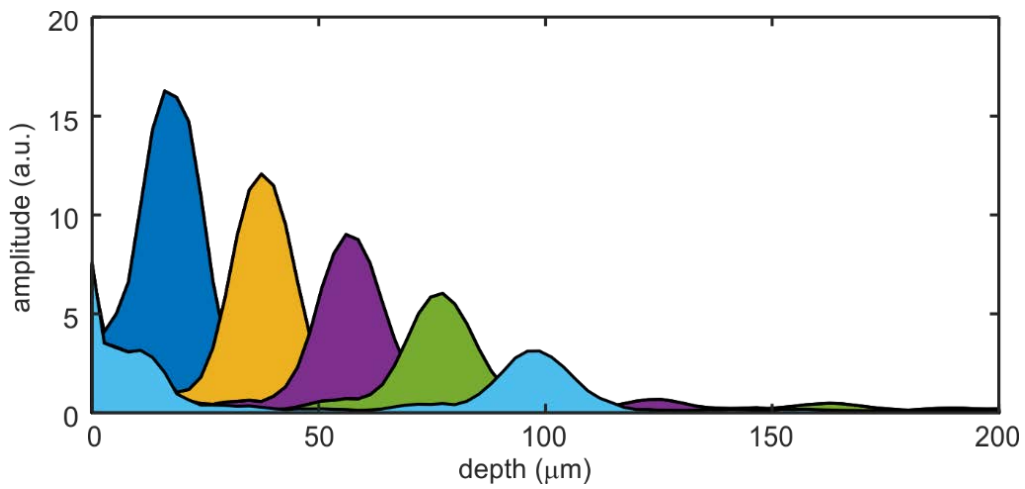


Fig 7.7 Fourier transform of the spectral intensity patterns along the line shown in Fig. 7.6. Each Fourier transform represents 10 $\mu$ m translation of the scanning mirror.

### 7.5.2 Two mirrors at different depths

In the previous case single mirror illuminates using a line source is axially translated with respect to the reference mirror. In the next set of experiments two axially separated mirrors (50 $\mu$ m separation) are laterally scanned by the line source (generated by the cylindrical lens and the slit). This is done to check the system's depth imaging capability in a single plane. Fig. 7.8a shows the recorded spectral interference pattern in the case of two axially separated mirrors as the object. Fig 7.8b shows the reconstructed intensity profiles at different depths for this object (25 lateral scans are used for the reconstruction).

Fig 7.8c shows the reconstructed intensity profile in the plane represented by the dashed rectangle in Fig. 7.8b. Here the vertical direction is the direction of the line source (object spatial information). The figure clearly shows that first the intensity corresponding, the reflection from mirror 2 comes to focus and, and then mirror 1 comes to focus indicating the depth discrimination capability of the system.

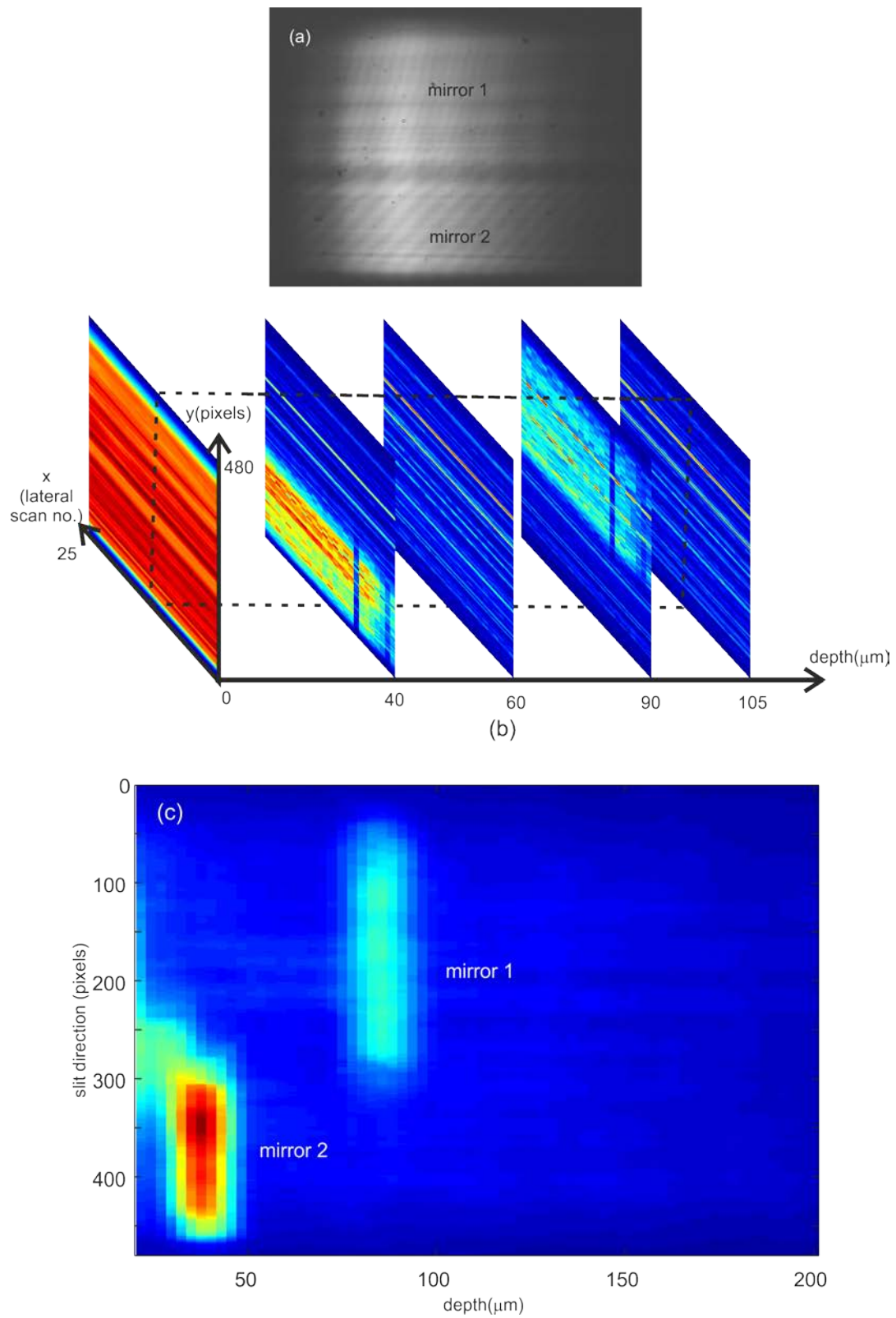


Fig 7.8 (a) Recorded spectral interference pattern with two axially separated mirrors as object. (b) Reconstructed intensity profile at various axial positions. (c) Intensity profile in the plane represented by the dashed rectangle in Fig. 7.8b, showing the positions of the two mirrors.

Depth discrimination is more evident while looking at the Fourier transform of the recorded spectral interference pattern at different lateral positions as shown in Fig. 7.9. Fig 7.9a is the interference pattern in frequency domain captured by webcam. Mirror 1 is placed approximately 50-275 pixels in vertical direction and Mirror 2 is placed approximately 320-450 pixels along slit. Fig 7.9b shows the Fourier transform of the spectral interference pattern along the red line in Fig. 7.9a, which provides the depth information about Mirror 1. Similarly, Fig. 7.9c shows the computed Fourier transform along the blue line shown in Fig. 7.9a, providing depth information of Mirror 2.

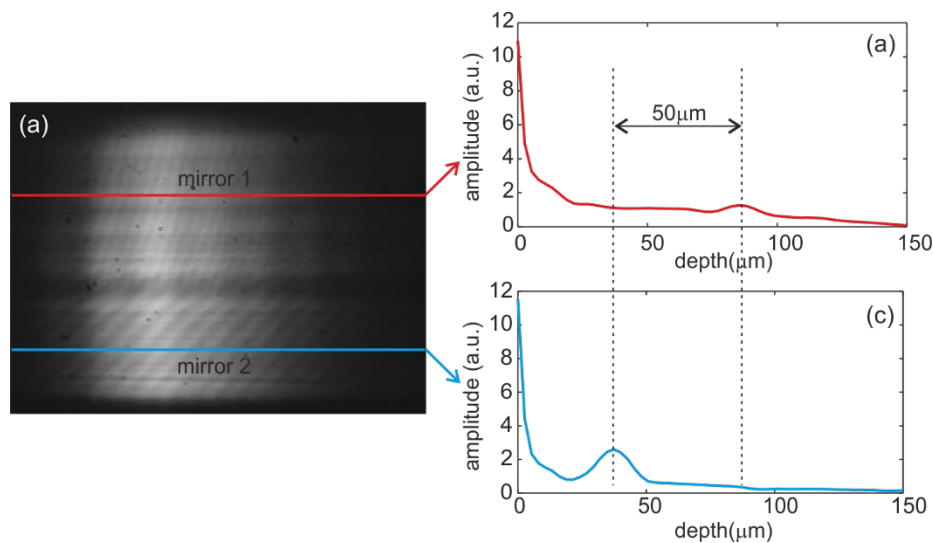


Fig 7.9 (a) Spectral interference pattern for two axially separated mirrors as object. (b) Fourier transform of the spectral interference pattern of the intensity variation along the red line providing depth information about Mirror 1. (c) Fourier transform of the intensity variation along the blue line providing depth information about Mirror 2.

### 7.5.3 Sample with multiple structures

In the previous sections, demonstrated the axial and lateral imaging capability of the system. In this section the experimental results in which a 3D object is scanned for reconstruction of depth information is described. The object is made up of three pieces of mirrors. A back coated mirror is placed at the front. Two holes are etched on this mirror at different lateral locations and two front coated mirrors are kept behind these holes at different axial distances from the first mirror to create two different depths and this object is scanned with 20 μm step size in lateral direction such that scanning can cover both the holes at different lateral locations. Fig. 7.10a to 7.10c shows the recorded spectral interference pattern for three different positions of the scanning beam (one each at the holes and one at the back coated mirror at the front). The Fourier transform along the lines shown in Fig. 7.10a to 7.10c is given in Fig. 7.10d to 7.10e respectively. It should be noted that these are representative Fourier transforms computed at a

position along the direction of the slit where the objects (holes) existed. The computed Fourier transforms show the depth discrimination of objects based on the spectral interference pattern. The reflection from back coated mirror is visible (Fig. 7.11a) at the depth of  $58\mu\text{m}$ . The intensity profile at each plane is obtained by combining the information from each lateral position of scanning beam. The two holes (marked object 1 and object 2) etched on the mirror are dark since they do not reflect much light (other than the diffracted light from the edges). The reflection of the light from the first mirror kept behind object 1 then becomes visible (Fig. 7.11d) at a depth of  $87\mu\text{m}$  and the reflection from the second mirror kept behind the back coated becomes visible at a depth of  $114\mu\text{m}$ . Fig. 7.11g shows the change variation in the reconstructed intensity with object depth.

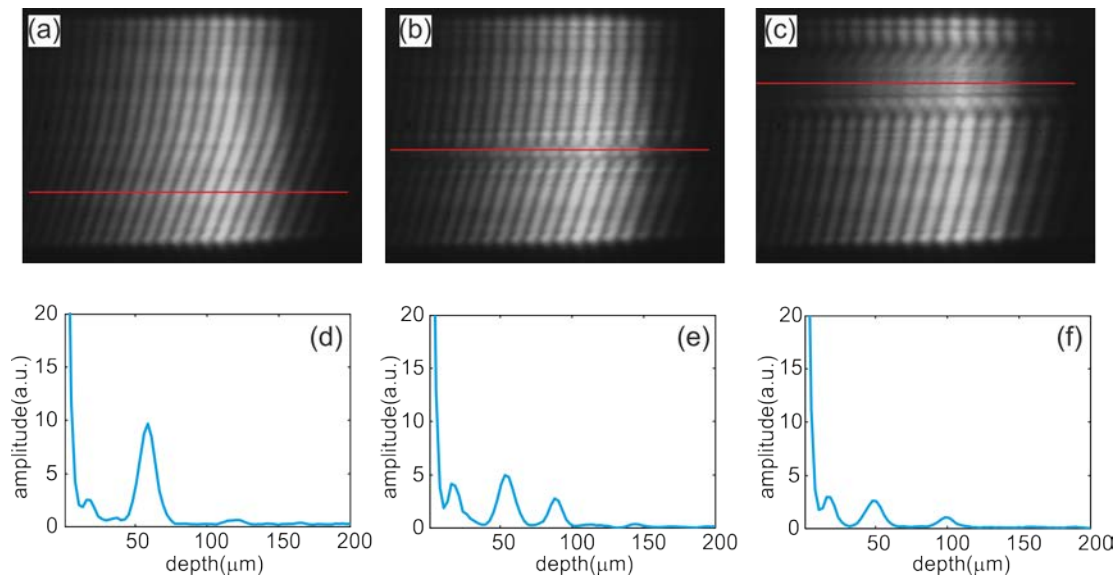


Fig 7.10 (a) Recorded interference patterns for different lateral positions of the scanning beam (a) reflection only from the back coated mirror. (b) reflection from back coated mirror and the first mirror behind it. (c) reflection from back coated mirror and second mirror behind it. (d) to (e) Fourier transform of the intensity variation along the lines shown in Fig. 7.10 (a) to (c) respectively.

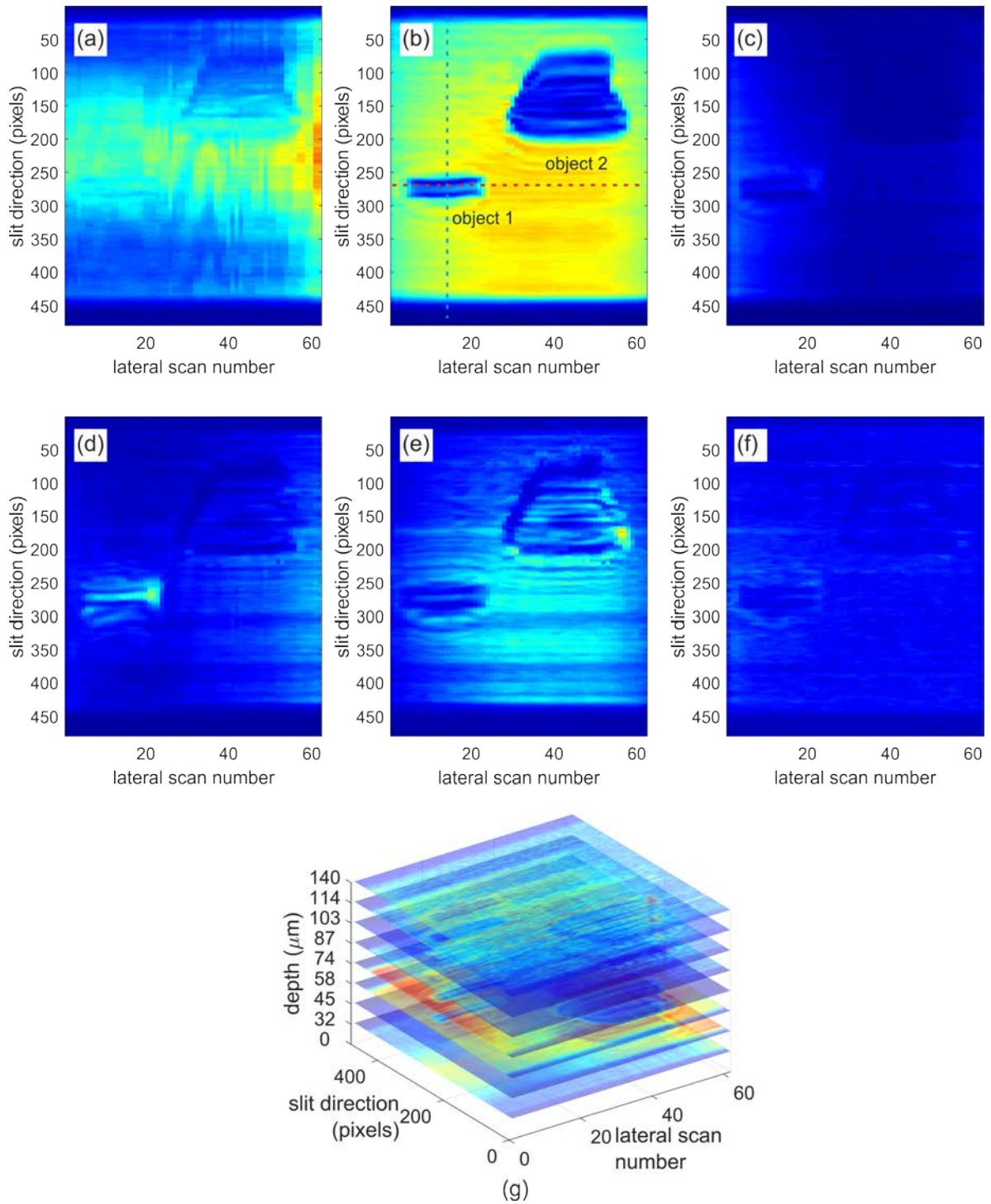


Fig 7.11 Reconstructed intensity from the Fourier transforms of the interference pattern for each lateral position of the scanning beam. (a) at depth 32 $\mu\text{m}$  (b) at depth 58 $\mu\text{m}$  (c) at depth 74 $\mu\text{m}$  (d) at depth 87 $\mu\text{m}$  (e) at depth 103 $\mu\text{m}$ , and (f) at depth 140 $\mu\text{m}$ . (g) Variation in reflected light intensity with depth

Fig. 7.12 shows the variation in intensity with depth along the lines shown in Fig. 7.11b. It shows the reflection from the first mirror behind object 1 (hole).

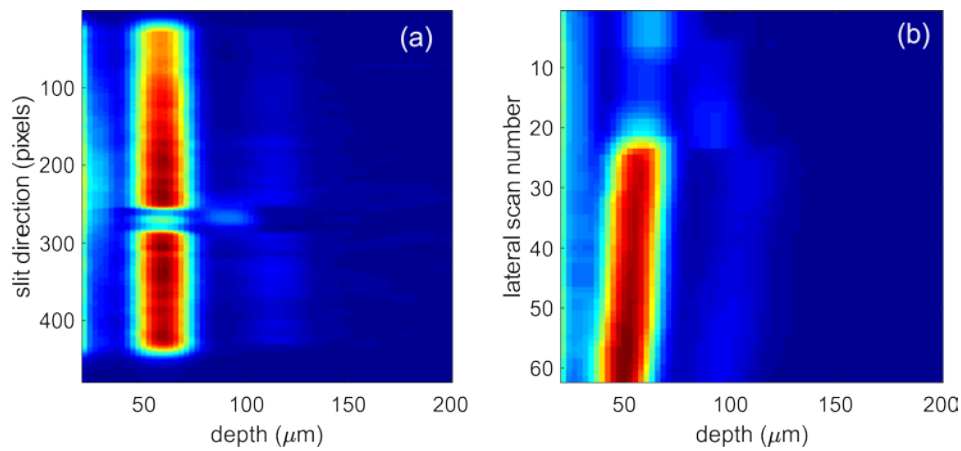


Fig 7.12 Reflected intensity with depth (a) along the dashed red line in Fig. 7.11b. (c) along the dashed blue line in Fig. 7.11b

## 7.6 Conclusions

A low-cost FDOCT system is demonstrated in this chapter. The FD-OCT system is developed employing a Light Emitting Diode (LED) owing to its relative simplicity, compactness, robustness and low cost, instead of Super luminescent Diode (SLD) that is the standard light source used in commercially available OCT devices. A webcam instead of a high-end CCD detector is used for recording of the spectral interference patterns. In the system demonstrated, several of the system parameters such as optical detection sensitivity is calculated which is found out to be nearly 30 dB. The axial resolution is found to be  $9\mu\text{m}$  and lateral resolution is  $12\mu\text{m}$  (depending upon the width of the scanning beam), while the maximum detectable depth  $z_{\text{max}}$  is  $288\mu\text{m}$ . For the proof of concept, is demonstrated by using mirrors as objects. In the future the system will be implemented using LED with higher power and different peak wavelengths to extend the maximum detectable depth of the system and realizing better axial resolution. Presently work is also under progress to investigate bio-samples using the technique.